

## Non-axisymmetric flow field in an axial impulse turbine

Byeung Jun Lim<sup>1</sup> and Seung Jin Song<sup>2,\*</sup>

<sup>1</sup>*Engine Department, KHP Development Division, Korea Aerospace Research Institute, 45 Eoeun-dong, Yuseong-gu, Daejeon 305-333, Korea*

<sup>2</sup>*School of Mechanical and Aerospace Engineering, Seoul National University, Seoul 151-744, Korea*

(Manuscript Received July 24, 2006; Revised July 13, 2007; Accepted July 16, 2007)

### Abstract

Phenomena such as hard landings or geometric flaws can cause non-axisymmetric tip clearance in turbines. Such geometric imperfections induce flow distortions which can, in turn, cause self-excited vibration of the rotor, or rotordynamic instability. Flow field perturbations in a single-stage, unshrouded impulse turbine caused by non-axisymmetric tip clearance have been investigated experimentally. Steady velocity and pressure data have been acquired at the design point with and without static turbine casing offset. Perturbations in tangential velocity and casing wall pressure have been obtained, and rotordynamic forces along and perpendicular to the axis of offset have been inferred. Compared to an unshrouded 20% reaction turbine, the forces due to tangential force asymmetry are much smaller, but the forces due to pressure asymmetry are comparable.

**Keywords:** Non-axisymmetric tip clearance; Flow induced vibration; Impulse turbine

### 1. Introduction

Turbomachinery vibration can be distinguished by the type of forcing as either forced or self-excited. A self-excited vibration occurs when the rotor's vibratory motion extracts energy from an external source such as the working fluid. This energy then adds to the vibratory motion, and this unstable phenomenon is called rotordynamic instability. Structural sources and fluid-structure interactions can cause rotordynamic instability. Many turbopump and gas turbine engine development programs were plagued by rotordynamic instability problems [1].

One major cause of rotordynamic instability has been attributed to the fluid excitation forces due to a non-uniform tip clearance gap. These forces arise when the whirling motion displaces the rotor center from the casing center position. Thomas first identified the problem in steam turbines [2], and Alford

independently identified the same problem in jet engines [3].

According to Alford, in a turbine with an offset shaft, the local efficiency and the local tangential force (i.e. torque) is assumed to be higher in the smaller tip gap region. When the torque distribution is integrated around the circumference, the net result is a force acting orthogonal to the displacement, which adds energy to the forward whirling motion (Fig. 1).

Most previous investigations have focused on the excitation forces due to static offsets [4-6]. Martinez-Sanchez et al. [7] obtained lateral excitation force and aerodynamic data in an unshrouded 20% reaction turbine with a statically offset rotor. Subsequently, Song acquired force data for the 20% reaction turbine and developed a theoretical model [8, 9].

However, most liquid rocket fuel turbo pumps use impulse (0% reaction) turbines to save weight. Since these impulse turbines have not yet been investigated, this study focuses on flow field redistribution due to non-axisymmetric tip clearance in an unshrouded axial flow impulse turbine.

\*Corresponding author. Tel.: +82 2 880 1667  
E-mail address: sjsong@snu.ac.kr  
DOI 10.1007/s12206-007-1020-y

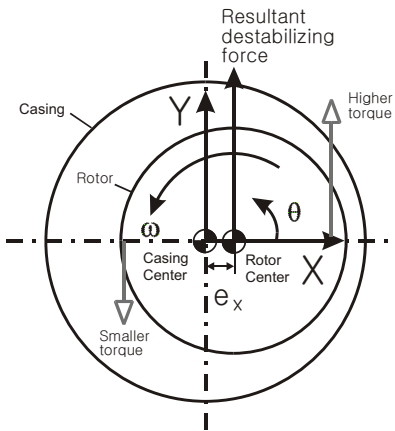


Fig. 1. Geometry of Alford's model.

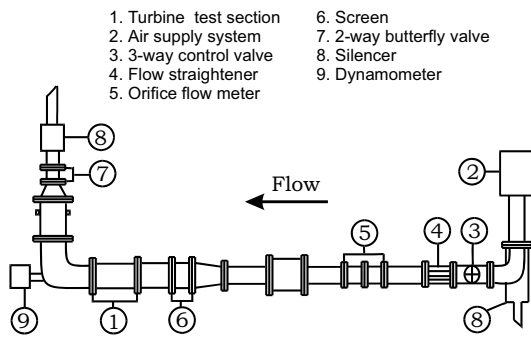


Fig. 2. Top view of experimental facility.

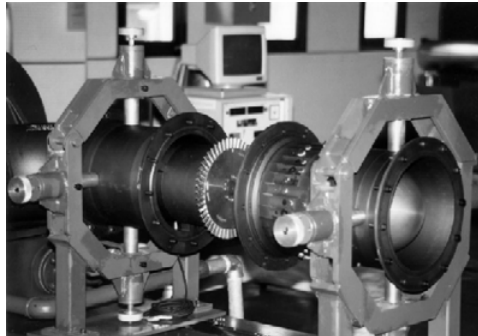


Fig. 3. Turbine test section.

## 2. Experimental facility

The experimental facility, which is located at the Korea Aerospace Research Institute (KARI) in Daejon, Korea, consists of the main flow loop and auxiliary systems. A detailed description is given in Oh et al. [10]. Fig. 2 shows the overall schematic of the experimental facility, and Fig. 3 shows a photograph

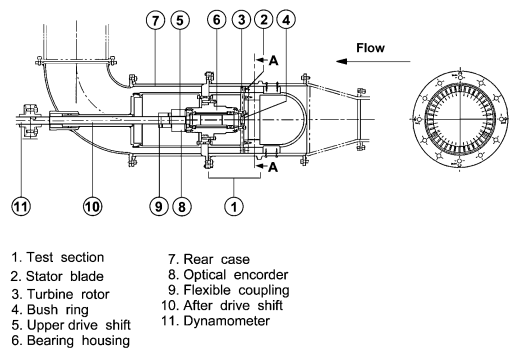


Fig. 4. Schematic of the turbine test section.

Table 1. Design parameters for the test turbine.

Parameters	Test Turbine
<b>Reaction</b>	0.0
Flow Coefficient	0.58
Work Coefficient	2.6
Stator Blade Exit Angle (deg)	73.0
Rotor Blade Inlet Angle (deg)	58.0
Rotor Blade Exit Angle (deg)	-58.0
Rotor Mean Radius (mm)	120.0
Rotor Blade Span (mm)	24.0
Rotor Blade Chord (mm)	12.5
Number of Blades (ea)	50
Mass Flow Rate (Kg/sec)	0.76
Inlet Axial Flow Velocity (m/sec)	30
Rotational Speed (rpm)	4001
Inlet Temperature (°K)	298

of the test section. The air supply system is composed of a 2-stage, centrifugal compressor powered by a 500-hp electric motor. The flow rate is controlled by a three-way control valve and a two-way butterfly valve. The rotational turbine speed is controlled by a dynamometer.

The turbine test section is designed to facilitate testing with both uniform (0.5 mm) and non-uniform tip clearances. The main components of rotating machinery are the turbine rotor, bush ring, and the upper drive shaft (Fig. 4). Static offset is obtained by mounting the test section casing eccentrically relative to the concentric rotating parts.

The test turbine is a 1:1 replica of an unshrouded impulse turbine stage used in an actual turbopump. The design flow and work coefficients are 0.58 and 2.6, respectively (Table 1).

Flow instrumentation is detailed in Fig. 5. The 3-hole probes at Stations 1 and 5 are traversed radially.

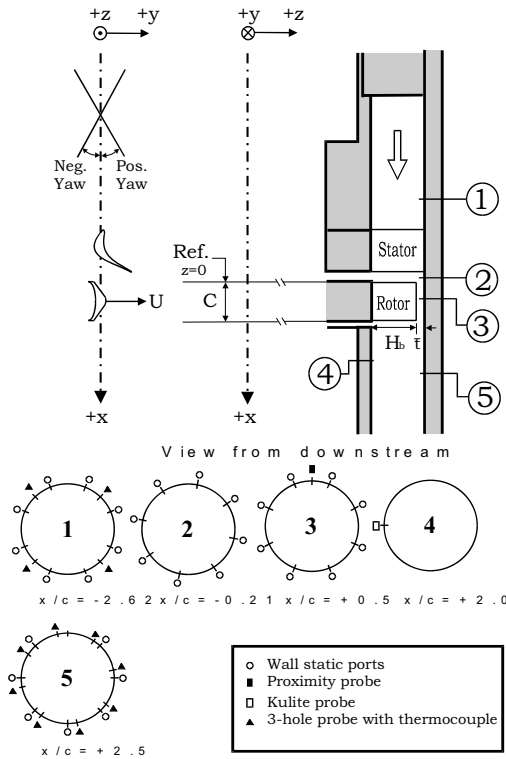


Fig. 5. Axial locations for aerodynamic instrumentation and types of instruments used at each section.

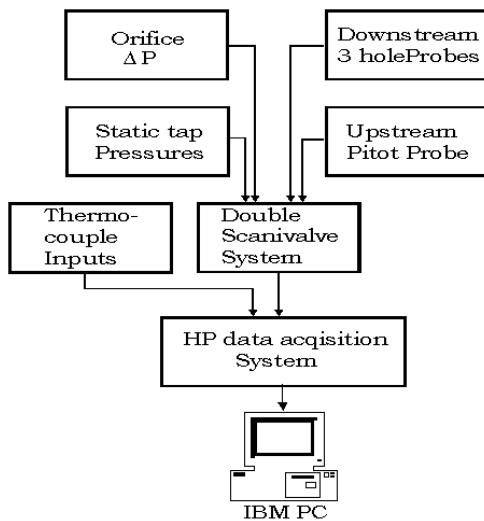


Fig. 6. Flow chart of the data acquisition scheme.

They sense axial and tangential velocity components, total & static pressures, and total temperature. Static pressure taps are located at all axial stations. All of the directional probe pressures, static wall tap pres-

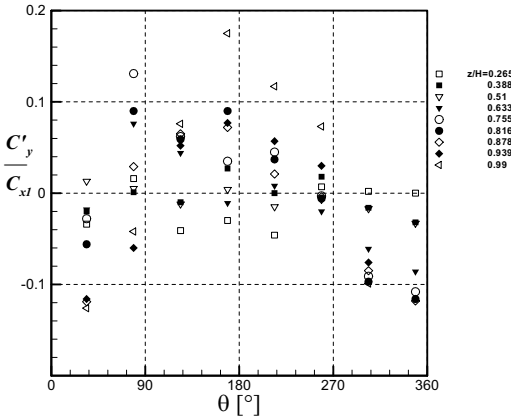


Fig. 7. Perturbation in tangential velocity vs. azimuthal angle at  $x/c=2.5$  ( $\Phi=0.58$ ,  $e/H_b=0.01 - e/H_b=0.00$ ).

sures, and the inlet probe pressures are routed through a Scanivalve multiplexer, and are measured with 1.25 and 12.5 psid pressure transducers. The transducers have an uncertainty of  $\pm 0.25\%$  of the full scale value.

The pressure and temperature data are transferred to a PC via HP E1413A automatic data acquisition/control system and HP 3456A digital voltmeter system. Fig. 6 shows the data acquisition flow chart.

### 3. Flow survey results

Data have been acquired under zero-offset (concentric) and static-offset (eccentric) conditions at the turbine design condition. At the design point, the rotational speed is 4000 rpm, and the mass flow rate is 0.76 kg/s.

Generally, directional probes are used to obtain steady state aerodynamic data. However, the downstream directional probes actually sense flows which are unsteady. To bound the error due to flow unsteadiness, the mass flow rate, inferred from the probe data at Station 5 ( $x/c=+2.5$ ), has been compared against that from the orifice flow meter. The mass flow rates match each other to within 5%.

Fig. 7 shows the azimuthal distribution of the perturbation in tangential velocity due to the rotor offset at Station 5 ( $x/c=+2.5$ ) at various radii ( $z/H_b$ ). The maximum gap is located at  $\theta = 180^\circ$ , and  $z/H_b$  values are 0 and 1 at the hub and casing wall, respectively. Tangential velocity is defined to be positive in the direction of rotation. Thus, at most radial locations the downstream flow is overturned in the bigger gap region ( $180^\circ$ ) and overturned in the smaller gap re-

gion ( $0^\circ$ ).

The tangential force exerted on the turbine blades by the fluid, per unit perimeter, is given by the Euler turbine equation as

$$f_y(\theta) = \int_0^H \rho c_x (c_{y2} - c_{y5}) dz \quad (1)$$

where  $c_{y2}$  and  $c_{y5}$  are the tangential velocities at the rotor inlet and exit, and  $\rho c_x$  is the mass flux at each azimuth. The perturbation in the tangential force caused by the rotor offset,  $f'_y(\theta)$ , is obtained by subtracting the concentric tangential force distribution from the eccentric data, and Fig. 8 shows the  $f'_y(\theta)$  plotted versus azimuthal angle. A tangential force deficit near the maximum gap is clearly visible. Such

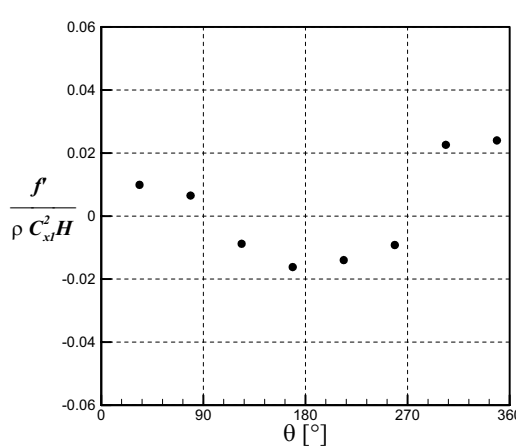


Fig. 8. Peturbation in tangential force extracted vs. azimuthal angle at  $x/c=2.5$  ( $\Phi=0.58$ ,  $e/H_b=0.01 - e/H_b=0.00$ ).

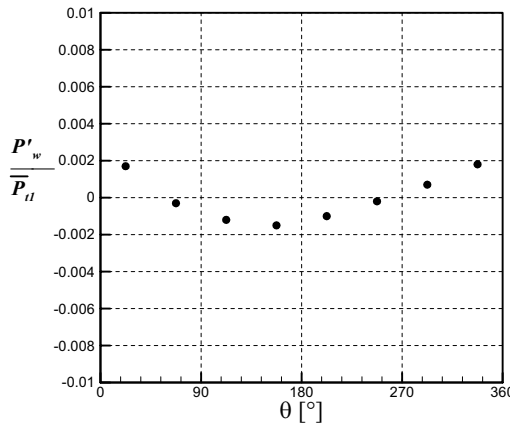


Fig. 9. Casing wall pressure perturbation vs. azimuthal angle at  $x/c=0.5$  ( $\Phi=0.58$ ,  $e/H_b=0.01 - e/H_b=0.00$ ).

a defect, which is the classic Alford mechanism shown in Fig. 1, would cause a forward whirl.

The lateral forces also arise due to non-axisymmetric pressure distribution. Fig. 9 shows the perturbation in the tangential pressure distribution after the concentric case has been subtracted from the eccentric case. The non-axisymmetric pressure has its minimum around  $150^\circ$ , and would also tend to excite a forward whirl.

These lateral forces due to flow asymmetries are then converted into nondimensional rotordynamic stiffness coefficients by taking the slopes of the curve of the forces vs. eccentricity. The direct stiffness coefficient ( $k_{XX}$ ) and the cross stiffness coefficient ( $k_{XY}$ ) are thus

$$k_{XX} = \frac{2F_x R}{Q(e/H_b)} \quad \& \quad k_{XY} = \frac{2F_y R}{Q(e/H_b)} \quad (2)$$

Such stiffness coefficients due to tangential force asymmetry and pressure asymmetry for both impulse and 20% reaction turbines are listed in Tables 2 and 3, respectively. The signs of the impulse turbine's rotordynamic stiffness coefficients are consistent with those of the 20% reaction turbine. Both  $f'_y$  &  $p'$  lead to a positive  $k_{XY}$ , which destabilizes the rotor into a forward whirl. Also, both  $f'_y$  &  $p'$  result in a negative  $k_{XX}$ , which tends to restore the rotor back to center. However, the magnitudes of the impulse turbine's  $k_{XX}$  and  $k_{XY}$  due to tangential force variation are merely 5% and 20% of those found in the 20% reaction turbine. As expected, since there is no flow expansion through the rotor in an impulse turbine, the asymmetry in rotor tip clearance does not result in significant tangential force asymmetry. On the contrary, the magni-

Table 2. The direct and cross stiffness coefficients for an impulse turbine.

Tangential force		Pressure		Total	
$k_{XX}$	$k_{XY}$	$k_{XX}$	$k_{XY}$	$k_{XX}$	$k_{XY}$
-0.03	0.48	-3.16	1.15	-3.19	1.63

Table 3. The direct and cross stiffness coefficients for a 20% reaction turbine [9].

Tangential force		Pressure		Total	
$k_{XX}$	$k_{XY}$	$k_{XX}$	$k_{XY}$	$k_{XX}$	$k_{XY}$
-0.6	1.9	-2.6	1.6	-3.2	3.5

tudes of the impulse turbine's  $k_{XX}$  and  $k_{XY}$  due to pressure asymmetry are 120% and 71% of those found in a 20% reaction turbine. The pressure perturbation is an indication of large length-scale, potential flow response to tip asymmetry, and this effect remains significant even in an impulse turbine.

#### 4. Conclusions

The following conclusions can be drawn from this investigation:

- (1) A long length scale flow field redistribution due to non-uniform tip clearance exists in an impulse turbine.
- (2) The directions of the impulse turbine's excitation forces are consistent with those of a 20% reaction turbine.
- (3) Compared to a 20% reaction turbine, the non-uniform tangential force effect is significantly decreased, but the non-uniform pressure effect remains in an impulse turbine.

#### Acknowledgment

The authors gratefully acknowledge support from the Micro Thermal System Research Center, BK21, and IAMD of Seoul National University; KARI; and Samsung Techwin.

#### Nomenclature

$c$	: Axial blade chord
$c_x$	: Axial velocity
$c_y$	: Tangential velocity
$e$	: Magnitude of rotor offset
$f_y$	: Tangential force acting on the rotor
$F_X$	: Lateral force in direction of the offset
$F_Y$	: Lateral force perpendicular to the direction of the offset
$H$	: Annulus height
$H_b$	: Blade span
$k$	: Nondimensional stiffness coefficient
$Q$	: Turbine torque
$R$	: Mean turbine radius
$U$	: Rotational speed
$X$	: Direction of minimum gap in the fixed coordinate system
$x$	: Axial direction
$Y$	: Direction of $\pi/2$ radius ahead of X
$y$	: Tangential direction

$z$	: Radial direction
$\phi = c_x/U$	: Turbine flow coefficient
$\theta$	: Azimuthal angle measured in the direction of rotation from the minimum gap location

#### References

- [1] E. C. Ek, Solution to the Subsynchronous Whirl Problem in the High Pressure Hydrogen Turbomachinery of the Space Shuttle Main Engines, AIAA/ASME /SAE 14 th Joint Propulsion Conference Las Vegas NV (1978) 1-24.
- [2] H. J. Thomas, Unstable Natural Vibrations of Turbine Rotors Induced by the Clearance Flows in Glands and Blading, Bull. De. L.A.I.M 71 No 11/12, (1958).
- [3] J. S. Alfords, Protecting Turbomachinery from Self-Excited Rotor Whirl, *ASME Journal of Engineering for Power*. (1965) 333-344.
- [4] K. Urlachs, Clearance Flow-Generated Transverse Forces at the Rotors of Thermal Turbomachines, NASA TM-77292 (1983).
- [5] R. Wohlrab, Experimental Determination of Gap-Flow Conditioned Forces at Turbine Stages, and Their Effect on the Running Stability of Simple Rotors, NASA TM-77293 (1983).
- [6] J. M. Vance and F. J. Laudadio, Experimental Measurement of Alford's Force in Axial Flow Turbomachinery, *ASME Journal of Engineering for Gas Turbines and Power*. 106 (1984) 585-590.
- [7] M. Martinez-Sanchez, B. Jaroux, S. J. Song and S. Yoo, Measurement of Turbine Blade-Tip Rotordynamic Excitation Forces, *ASME Journal of Turbomachinery* 117 (3) (1995) 384-392.
- [8] S. J. Song and M. Martinez-Sanchez, Rotordynamic Forces Due to Turbine Tip Leakage: Part I - Blade Scale Effects *ASME Journal of Turbomachinery* 119 (4) (1997) 695-703.
- [9] S. J. Song and M. Martinez-Sanchez, Rotordynamic Forces Due to Turbine Tip Leakage: Part II - Radius Scale Effects and Experimental Verification *ASME Journal of Turbomachinery* 119 (4) (1997) 704-713.
- [10] S. H. Oh, S. J. Song and Y. S. Hong, An Experimental Facility Design to Determine Rotordynamic Coefficients due to Tip Clearance Asymmetry in Axial Turbines, 97-AA-018 ASME Asia '97 Singapore (1997).